Available online at www.sciencedirect.com
SCIENCE DIRECT
Talanta 68 (2006) 1623–1631
Talanta
www.elsevier.com/locate/talanta

FIB, TEM and LA–ICPMS investigations on melt inclusions in Martian meteorites—Analytical capabilities and geochemical insights

Davide Bleiner[a,*], Michele Macrì[b,c], Philippe Gasser[d], Violaine Sautter[b], Adriana Maras[c]

[a] *Universiteit Antwerpen, Department of Chemistry, Universiteitsplein 1, 2610 Wilriijk, Belgium*
[b] *Laboratoire de Minéralogie (USM 201) & CNRS UMR 7160, Museum National d'Histoire Naturelle, 61 rue Buffon, 75005 Paris, France*
[c] *Università degli Studi di Roma La Sapienza, Department of Earth Sciences, P.le Aldo Moro, 00185 Rome, Italy*
[d] *EMPA, Div. Concrete and Construction Chemistry, Überlandstrasse 129, 8600 Dübendorf, Switzerland*

Received 11 April 2005; received in revised form 27 July 2005; accepted 9 August 2005
Available online 23 September 2005

Abstract

In order to obtain full information coverage on melt inclusions in Martian meteorites (subgroup nakhlites) complementary micro-analytical techniques were used, i.e. focused ion beam, transmission electron microscopy and laser ablation. Using focused ion beam several lamellae for transmission electron microscopy were prepared and secondary electron images of cross-sections could be acquired. Laser ablation–inductively coupled plasma mass spectrometry analyses were performed on selected inclusions to obtain mass-oriented bulk composition of inclusions at depth. The differences in composition between melt inclusions in olivine and augite crystals would suggest a xenocrystic origin for olivine. Furthermore, electron diffraction patterns clearly indicated that the SiO_2-rich phase in inclusions from augite in meteorites from Northwest Africa site is re-crystallized, whereas it is still vitreous in the inclusions from Nakhla sampling site. Therefore, different post-entrapment evolutions were active for the two nakhlite meteorite sets, the Nakhla and the NWA817 set. Melt inclusions in Nakhla olivine presented alteration veins, which were presumably produced before their landing on Earth. If this is the case, this would indicate a alteration stage already on Mars with all the consequence in terms of climate history. Melt inclusions in Nakhla augite resulted unaffected by any alteration or modification following the entrapment, and therefore represent the best candidate to indicate the pristine magma composition.

Keywords: Focused ion beam (FIB); Transmission electron microscopy (TEM); Laser ablation–inductively coupled plasma mass spectrometry (LA–ICPMS); Melt inclusions; Shergotty Nakhla Chassigny (SNC) meteorites

1. Introduction

The recent space missions on planet Mars have raised lots of interest and attention on the geological history of the red planet. The access to direct analytical determinations on Martian samples will give a significant contribution to our understanding, which so far was mostly based upon indirect information. Of the approx. 24,000 meteorites that have been discovered on Earth, just 34 have been identified as originating from the planet Mars. These were originally discovered in three worldwide localities, namely *S*hergotty (India), *N*akhla (Egypt), and *C*hassigny (France), and they form the so-called SNC meteorite group. These meteorites are a set of Martian igneous rocks released into space as a consequence of large impacts, providing unique direct sampling of the bedrock of Mars. The provenance of the SNC meteorites has been long debated in the past, but nowadays their origin from Mars is well accepted. This is based on their petrological, geochemical, and geo-chronological characters [1–4]. The nakhlite subgroup [5] is retained to originate from the same cooling magmatic pile. These rocks are clino-pyroxenites consisting in predominant augite and minor olivine. Augite is an important rock-forming mineral in many igneous rocks, especially in gabbros and basalts, and it is also found in some hydrothermal metamorphic rocks. Augite is a part of an important solid solution series of the clino-pyroxene group. Olivine is the common name for a suite (solid solution) of iron–magnesium

* Corresponding author.
E-mail address: davide.bleiner@ua.ac.be (D. Bleiner).

0039-9140/$ – see front matter © 2005 Elsevier B.V. All rights reserved.
doi:10.1016/j.talanta.2005.08.022

silicate minerals known to crystallize first from a cooling magma rich in Fe and Mg and to weather first in the presence of water into clays or iron oxides. The occurrence of olivine on the surface of Mars and its susceptibility to chemical weathering has kept geochemists busy investigating how long it has been there and what that means about climate history. Studies on the magmatically coherent set of SNC meteorites, i.e. the nakhlite subgroup, contribute to the understanding of the thermodynamic and chemical evolution of the magmatic processes that have been acting on Mars.

In such geological samples a wealth of information is held within melt inclusions. Melt inclusions are formed from 1 to 500 μm drops of pristine magma trapped upon cooling in a growing mineral at different evolution stages. Melt inclusions can be found at different positions within the mass of a host phase. However, it is only those located at a certain depth within the host phase and not crossed by fractures that might have entirely preserved their pristine chemical integrity. In fact, provided that the trapping process isolated the melt from the rest of the evolving magma, this process froze valuable information that can be extracted later on.

It should be pointed out, that the origin of the mineral olivine in nakhlite meteorites has been debated, namely whether such a mineral is to be considered generated in situ within the cooling magma that originated the nakhlites (phenocrystal) or whether it crystallized elsewhere in the molten magma and migrated into the entrapment site later (xenocrystal) through the molten mass. In the latter case, olivine should not be considered in the mass balance when trying to calculate the composition of the original nakhlite magma. On the other hand, augite was definitely formed in situ. Thereafter, a comparison between the melt inclusions, i.e. pristine magma, found in augite and in olivine can be helpful to unravel this debate and shed new light on the petrogenesis of Mars.

The traditional analytical approach for melt inclusion study is represented by re-homogenization experiments, in which one investigates the phase equilibria upon re-heating the sample under the assumption of no external contamination of the re-homogeneized mass, in order to obtain insights on the crystallization sequence and magmatic composition. However, Varela et al. [6] performed re-homogenization experiments on melt inclusions in augite of nakhlite meteorites and obtained too much compositional variation of the end product to be representative of a parental magma.

Thereafter, in order to obtain more robust insights into the elemental composition of a set of melt inclusions, beam-assisted analytical techniques are preferred. For instance, Harvey et al. [7] and Treiman [8] investigated several melt inclusions in nakhlite meteorites by means of electron probe micro-analysis (EPMA). Unfortunately, they estimated that the average inclusion analysis should be related for just 72% to the inclusion own composition and the remaining 28% was to be attributed to the host mineral. A critical aspect in direct melt inclusions micro-analysis is the ability to measure the composition of the inclusion without any contribution from the host mineral. Often EPMA measurements on buried inclusions suffer from the contribution from embedding sample portions, because the measurement is volume-oriented. This means that the obtained concentration is related to the average count rate from the probed sample volume, the so-called excitation pear. This approach becomes especially limiting with small inclusions disseminated in the host phase, as observed in Ref. [8], or with measurements at the inclusion's margins, where in both cases the host is significantly contributing to the overall detected analytical signal.

Therefore, the ideal analytical technique for melt inclusion micro-analysis should offer high spatial resolution combined with the ability to extrude portions of the samples that might interfere with the direct measurement of the inclusion. Such "portions to be extruded" are meant to be either the host mineral as explained above or also potential heterogeneities and cavities within the sample itself. This means that the ideal analytical technique should offer a mass-oriented determination, instead of a volume-oriented one. Thus, it is mandatory to implement destructive analytical techniques, in order to be able to: (i) access the inclusion after excavation of the host; (ii) integrate the inclusion signal in direct relation to the effective mass that produced it; (iii) acquire the signal in depth resolved mode so that one is able to assess the occurrence of cavities or heterogeneities.

However, the use of destructive microprobes should be done in combination with an image survey of the samples. In fact the geometrical features of a melt inclusion are often more complex than the idealized spherical shape, and the volume of the inclusion might contain voids or pockets. This can make the excavation process risky, where the risk is that of destroying the sample without finally accessing to information-rich portions. Moreover, fundamental information on the mechanism of the minerogenesis processes can be obtained from the visual analysis of the geometrical relations among the phases, which therefore turns out to be important.

Aim of this work was the development of an efficient analytical operating procedure for our Martian meteorite samples, which are precious in both economic and scientific terms. The capabilities of three beam-assisted micro-analytical techniques were complementarily implemented, in order to obtain full information coverage, i.e. image documentation, crystallinity, and elemental composition. Initially focused ion beam (FIB) was used, which represents a recent advance of micro-beam technology. The use of FIB for melt inclusion studies is a novel approach to obtain micro-controlled preparation of the meteorite samples. Time-consuming and less accurate traditional manual procedures were thus overcome. FIB allowed the cross-sectional study of melt inclusions' structure as well as the preparation of plane-parallel lamellae (approx. thickness 100 nm) for transmission electron microscopy (TEM). TEM was implemented in a further investigations stage, in order to obtain information on inclusion geometry (secondary electron images), crystallinity features (electron diffraction patterns), elemental composition (EDX detection). As known, the potential of TEM is strongly a function of sample preparation, e.g. thickness over

the investigated domain. FIB micro-machining gave access to high resolution TEM data. To obtain validation of elemental composition, laser ablation–inductively coupled plasma mass spectrometry (LA–ICPMS) was used, which offered direct access to elemental and trace composition of solids. By pulsed ablation and online mass spectrometric determination of the ablated mass, melt inclusions located at depth could be reached and ablated directly without any signal mixing with the host mineral, since the spot size was carefully chosen to ablate the inclusion only. The latter is a significant advantage compared to EPMA because in LA–ICPMS by use of an internal standard one is able to correct for signal fluctuation, i.e. the ablation yield, in the presence of hollows. Alternatively in the presence of enriched pockets in the ablated inclusion, one can verify if changes in one element's signal integrals are due to local changes in composition or simply to the ablation yield. A further advantage of LA–ICPMS against EPMA is the fact that the elemental sensitivity is not a function of inclusion depth. In EPMA, due to absorption in the shallower regions, the measurement of an inclusion deep inside the host can be problematic because of lack of sensitivity. Furthermore, with LA–ICPMS one is able to localize potential voids or enrichment pockets in a depth-resolved mode after the ablation time is calibrated against the ablation depth. In fact, differently to other techniques like for instance secondary ion mass spectrometry (SIMS), LA–ICPMS' ablation yield is not severely affected by the change in silicatic mineral phase. In fact, since the laser sampling and the ICP–MS determination are separated in space, matrix effects are not relevant. This permitted to reliably match ablation depth and ablation time with a depth resolution in the micron range. LA–ICPMS for melt inclusion study is already well established. Taylor et al. [9] applied LA–ICPMS for the in situ analysis of silicate melt inclusions, stressing the advantages of using UV laser radiation for improved micro-sampling and small spot focusing. More recently Halter et al. [10] presented a comparison of four different quantification approaches using LA–ICPMS. In fact, considering that host mineral might be co-ablated with the inclusion, deconvolution of the mixed signal by an internal standard would be required. The authors suggested quantification through critical assessment of the whole rock differentiation trends. Concerning the quality of the quantitative determinations, Pettke et al. [11] presented a comparison among LA–ICPMS, EPMA and SIMS for melt inclusion analysis, suggesting that comparable results can be obtained provided the use of an appropriate internal standard. In Heinrich et al. [12] an extensive review of the use of LA–ICPMS in the geosciences is given.

2. Experimental

The Museum of Natural History of Paris and the CNRS "Theodore Monod" consortium provided the meteorite samples, whereas further samples were donated from a third party (J. Strobe). Thin sections from two different meteorite samples were investigated: double-polished sections of nakhlite meteorites (from Nakhla, Egypt) and double-polished sections of NWA817 meteorites (from Northwest Africa). Double-polished sections were prepared using first silicon carbide 320 and 600 then diamond D_p-spray of 3 and 1/4 μm; samples were finally cleaned with *o*-xylene. Double-polished sections are preferred to normal petrographic thin sections to study melt inclusions, since they allow observations in the third dimension.

The samples were micro-machined with a Strata DB 235 dual beam FIB workstation (FEI company, USA). The instrument incorporates together with the FIB Ga^+ column a scanning electron microscope (SEM) column tilted to each other at an angle of 52°. The FIB column is adjustable from 1 pA to 20 nA at 30 kV with a specified resolution of 7 nm, as reported by the manufacturer. The instrument is equipped with four secondary electron and ion detectors for image acquisition. The workstation has a digital patterning generator and four gas injection systems (GIS) for deposition and specific etching processes. The TEM samples were prepared by milling down to an electron-transparent sample (i.e. 100 nm thick) out of a bulk sample including the melt inclusion of interest. TEM observations and analyses of the lamellae were performed with a JEOL 200FX TEM operated at 200 kV.

Melt inclusions in Nakhla olivine and clinopyroxene were analyzed using a Nd:YAG laser ablation system (Quanta-Ray DCR-11, Spectra-Physics) in-house modified to obtain the fourth harmonic (266 nm) for improved micro-sampling. The details of the EMPA facility modifications are presented elsewhere [13]. The laser was operated at 10 Hz, with pulse energy of 4 mJ resulting in a fluence of 50 J/cm^2. The laser beam was focused with a $f = 40$ mm plano-convex lens, which led to a depth of focus of 1–2 mm depending on the spot size. This distance was much longer than the ablated depth, thus constant irradiation conditions was produced throughout the entire measurement time. A pinhole was used to control the spot size, by imaging it onto the sample surface. The use of a size-varying pinhole for controlling the spot size ensured that the ablation efficiency was comparable at all spot sizes (comparable fluence), since the beam was truncated so that the energy-to-surface ratio was constant. This was valid because of homogeneous irradiation of the pinhole. Thus, comparable results were obtained for all inclusions regardless their size and the overall integrated signal by using internal standards. The ablation cell was 30 cm^3 with a 0.5 mm i.d. inlet nozzle to ensure a steady gas jet. The transport tube was a 4 mm i.d. and 1.5 m long PVC tube. Helium was used as carrier gas at a flow of 0.6 L/min. The ICP–MS was a quadrupole plasma-mass spectrometer (PE/Sciex Elan 6000) operated under standard conditions. A menu of 20 isotopes was edited, for the elemental analysis of Na, Si, Ca, Ti, Mn, Fe, Cr, Al, Mg, Ni, La, REE. Background signal was monitored both off-peak at mass 220.5 and on-peak for 20 s previous the operation of the laser on the analytes mass. Detection limits were in the 0.1–10 mg/kg range depending

on the elemental sensitivity, yet several orders of magnitude below the expected concentrations in the samples. Internal precision, i.e. point-to-point intensity scatter of one individual LA–ICPMS time-dependent signal, was below 10% and it was mostly due to the pulsation of the laser beam, to the pulse energy stability, and the fluctuation of the aerosol transport to the ICP–MS. External precision, i.e. the reproducibility of individual integrals, was around 5%, depending on the isotopic abundance and elemental concentration as dictated by counting statistics. For the sake of calibration, three standard reference materials (SRM) were used. Two SRM's were commercially available certified reference materials from the National Institute of Standards and Technology (NIST 610, NIST 612). A third SRM was a norm clinopyroxene that had been also characterized by electron probe microanalysis (EPMA). The quantification procedure for melt inclusions using LA–ICPMS has been discussed in detail in a previous work [12].

3. Results and discussion

Fig. 1 shows few steps of FIB-assisted micro-machining for the preparation of one sample thin lamella. A surface of approx 20 μm × 10 μm was previously marked after optical microscopy investigation in transmitted light as characterized by the presence of melt inclusions. This procedure was important because the FIB facility permits to observe the surface only, using the SEM column. Two pits were dug so that at each raster cycle the wall in-between, i.e. the prepared lamella, became thinner and thinner. Panel (a) shows a top view whereas panel (b) shows an oblique view during the milling process. In panel (c) the sample preparation is completed and the lamella needs just to be separated at the margins. The end thickness of approx. 100 nm is shown in panel (d), which offers a top view of the processed area.

Fig. 2 shows a secondary electron (SE) image of two lamellae, which permits to view a cross-section of the melt

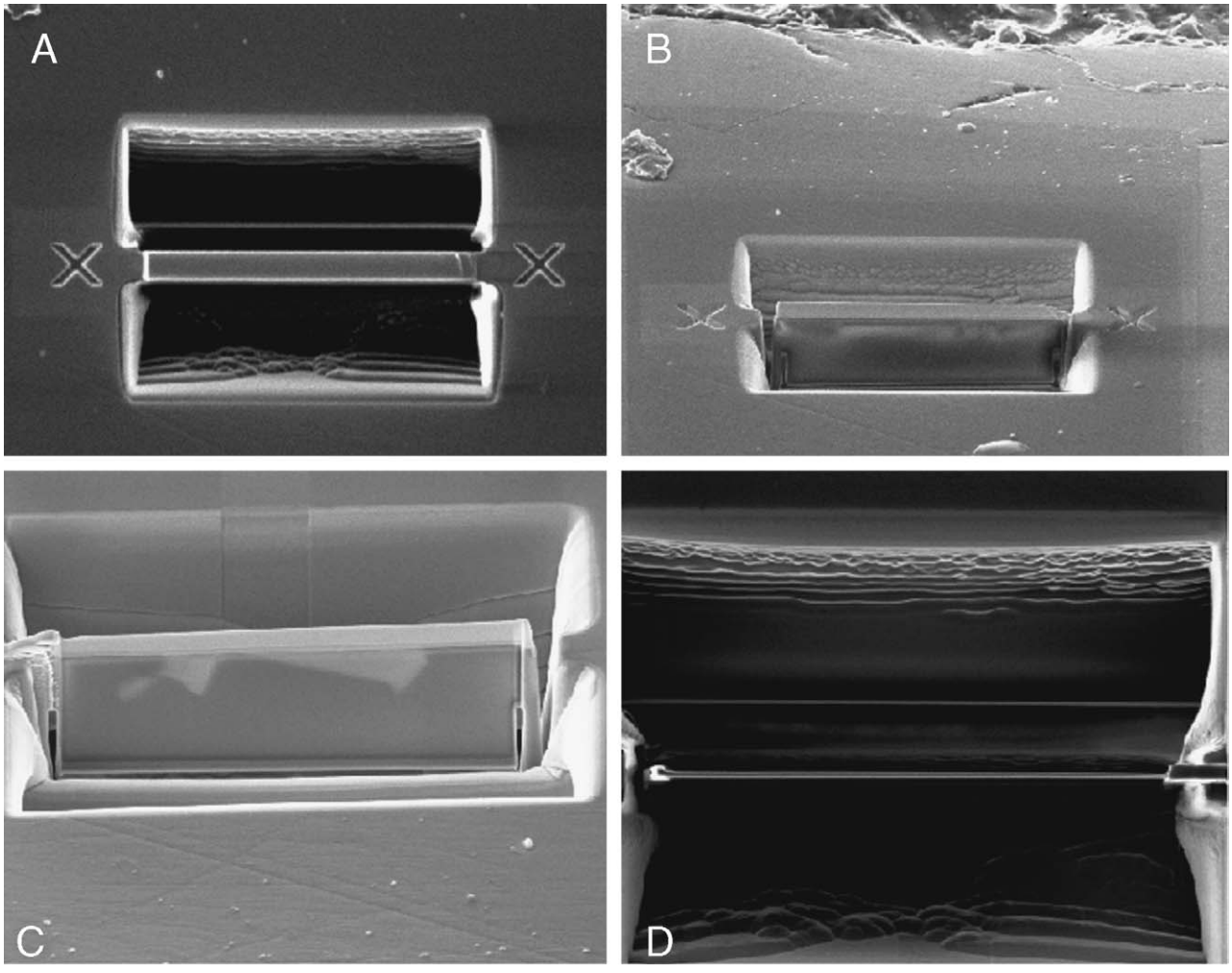

Fig. 1. Secondary electron images of the FIB-assisted lamellae preparation. (A) Two pits of size 20 μm × 5 μm are dug close to each other in the melt inclusion area (top view). (B) The wall between the pits is thinned out down to 100 nm thickness (oblique view). (C) The lamella is being cut at the edges. (D) Top view of the finished 100 nm lamella.

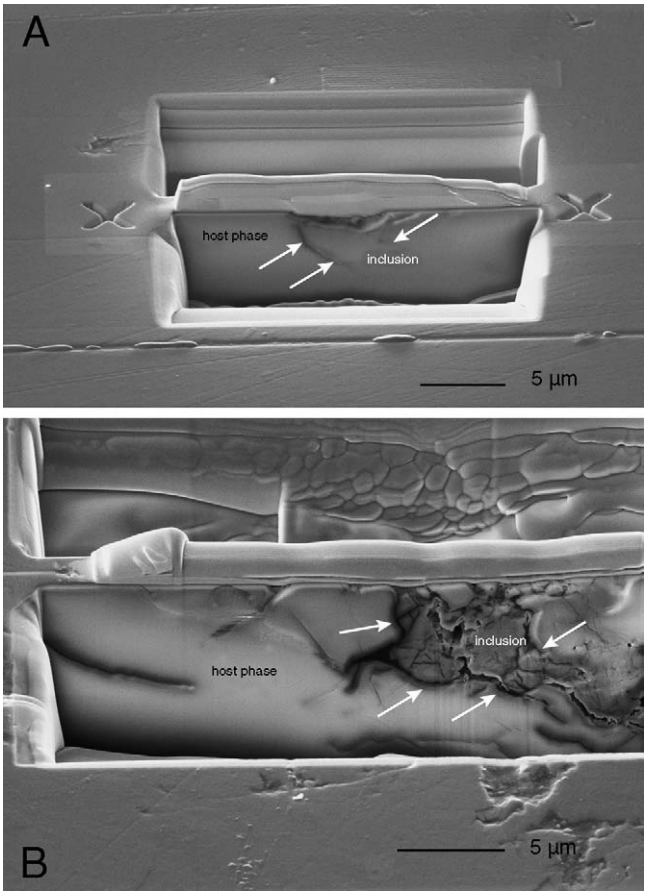

Fig. 2. SEM images of excavated sample using FIB, and melt inclusions structure. (A) Nakhla sample showing melt inclusion in augite of eye-like shape buried with oblique axis relative to the sample surface. (B) NWA817 sample and relative melt inclusion in augite, characterized by an irregular shape and occurrence of cavities.

inclusions in the Nakhla and NWA817 sample, respectively. The melt inclusion edges are indicated by the arrows. The shape of the inclusion in Fig. 2(A) is eye-like with an oblique elongation axis with respect to the sample surface, and gauge of a few microns. Fig. 2(B) shows a large trench in the NWA817 sample, which clearly visualizes the complex melt inclusion structure. One notes the extremely irregular shape and the occurrence of cavities and fractures. The inclusions were multiphase.

The presence of fractures permitted to formulate analytical and geochemical considerations. First, the occurrence of cavities influences the measurement when using volume-oriented analytical techniques, e.g. EPMA. If one is not aware of the actual mass of the inclusion, and has no fully matrix-matched reference material to control the signal yield per unit mass, the quantification algorithm might erroneously re-calculate the raw data and output misleading results. Secondly, the presence of fractures would suggest that such inclusions have undergone alteration, presumably losing their pristine characters. Due to the fact that these were inclusions buried deep inside the host mineral, it is likely that such alteration process was produced by early fluids circulating within the rock, instead of by tardive surface atmospheric weathering, i.e. long before the sample was relocated on the Earth as a meteorite.

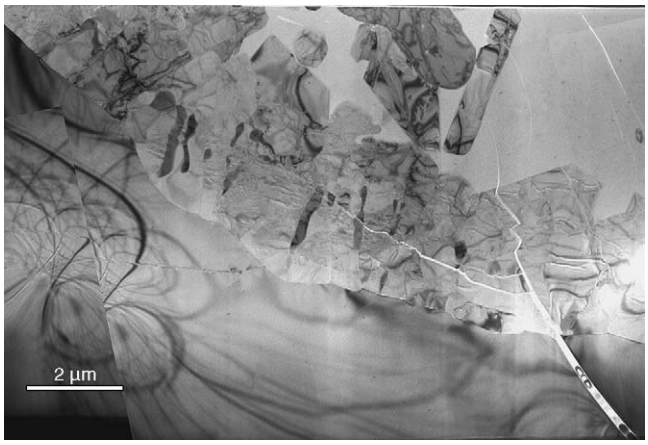

Fig. 3. TEM image of FIB-prepared lamaella where the TEM–EDX determinations have been performed (Table 1). Nakhla melt inclusion in clinopyroxene with transverse pockets of opaque minerals (Fe–Cr oxides) and tardive fracture with fillings.

Fig. 3 shows a close-up of one Nakhla lamella that visualizes the structure of the melt inclusion. One sees the occurrence of Fe–Cr oxides sub-inclusions in transversal elongated opaque pockets. On the right side one also notes the occurrence a bifurcated fracture with secondary fillings. The fact that such a fracture cuts through the opaque minerals indicates that the oxide phases are temporally antecedent. Table 1 summarizes TEM–EDX composition of rock-forming phases in this sample.

Fig. 4 shows another nakhlite lamella where a chloro-apatite crystal could be found in a clinopyroxene host. The chloro-apatite crystal could develop its crystallographic habit within the embedding host mass that therefore had to be still molten. Due to the possibility of preparing TEM lamellae with parallel faces over the whole sample area the quality of the TEM acquisition is now higher than what could be obtained with traditional sample preparation methodologies. Table 2 summarizes TEM–EDX composition of rock-forming phases here.

Fig. 5 shows a FIB lamella prepared from the NWA817 meteorite. Here one sees again the occurrence of cavities as well as the presence of Fe-bearing daughter minerals (i.e. hedenbergite, fayalite and chloro-apatite) and veins of alteration. Table 3 summarizes TEM–EDX composition of rock-forming phases occurring in this sample.

The sample lamellae were characterized by means of TEM–EDX as shown in Tables 1–3 (host phases, with most geochemically significant values) as well as using selected area electron diffraction (SAED) where it was significant to determine whether the mass was crystalline or vitreous. The nakhlite samples showed inclusions in both the clinopyroxene and the olivine. The clinopyroxene showed compositional

Table 1
Normalized concentration in mass percent of rock-forming phases in a selection of points determined using TEM–EDX in Nakhla sample of Fig. 3

Phase	Silica-rich phase				Clinopyroxene					
	1	2	3	4	1	2	3	4	5	6
SiO_2	79.5	80.4	86	89	52.8	44.6	55.8	54.1	54	54.6
Al_2O_3	15.8	11.8	8.7	4.2	<	<	<	0.3	0.2	<
Fe_2O_3	2.4	4.2	3.5	2.4	34.5	41.3	15.8	17.2	17.7	25.9
MgO	<	<	<	<	11.0	10.4	8.6	7.9	7.9	8.0
CaO	0.1	<	0.5	0.4	1.7	3.7	19.5	20.1	19.8	11.5
MnO	<	<	<	<	<	<	0.3	0.4	0.4	<
Na_2O	2.2	3.5	1.2	4.0	<	<	<	<	<	<
K_2O	<	<	<	<	<	<	<	<	<	<

Phase	Cl-apatite	Olivine	Fe–Cr Oxides				
	1	1	1	2	3	4	5
SiO_2	3.4	31.4	<	<	<	<	<
TiO_2	<	<	<	<	<	0.2	0.2
Al_2O_3	<	<	<	<	<	<	<
Fe_2O_3	2.5	58.5	88.4	87.7	89.0	88.0	87.0
Cr_2O_3	<	<	11	11.5	10.5	11.2	12.5
MgO	<	9.1	<	<	<	<	<
CaO	54.4	0.3	<	<	<	0.6	0.3
MnO	<	0.7	0.6	0.8	0.5	<	<
Na_2O	<	<	<	<	<	<	<
K_2O	<	<	<	<	<	<	<
P_2O_5	37.9	<	<	<	<	<	<
Cl_2O	1.8	<	<	<	<	<	<

The numbers 1, 2, 3, 4, 5, and 6 in the header denote the analysis number.

Table 3
Normalized concentration in mass percent of rock-forming phases in a selection of points determined using TEM–EDX in NWA817 sample of Fig. 5

Phase	Silica-rich phase						
	1	2	3	4	5	6	7
SiO_2	90.1	85.9	87.7	73.0	88.2	87.6	89.0
TiO_2	<	<	<	<	<	<	<
Al_2O_3	9.0	12.6	9.7	19.7	9.3	11.4	10.4
Fe_2O_3	<	<	<	<	<	<	<
Cr_2O_3	<	<	<	<	<	<	<
MgO	<	<	<	<	<	<	<
CaO	0.9	1.5	1.0	3.1	1.0	1.0	0.6
MnO	<	<	<	<	<	<	<
Na_2O	<	<	1.5	4.3	1.4	<	<
K_2O	<	<	0.1	<	<	<	<

Phase	Clinopyroxene		Olivine			Cl-apatite	
	1	2	1	2	3	1	2
SiO_2	49.4	54.3	21.7	26.4	26.1	2.6	1.8
TiO_2	<	<	<	<	<	<	<
Al_2O_3	<	<	<	<	<	<	<
Fe_2O_3	36.3	16.5	77.5	72.7	73.3	<	<
Cr_2O_3	<	<	<	<	<	<	<
MgO	<	8.8	<	<	<	<	<
CaO	13.9	20.3	<	<	<	54.9	54.2
MnO	0.4	<	0.8	1.0	0.7	<	<
Na_2O	<	<	<	<	<	<	<
K_2O	<	<	<	<	<	<	<
P_2O_5	<	<	<	<	<	38.0	40.0
Cl_2O	<	<	<	<	<	4.5	4.0

The numbers 1, 2, 3, 4, 5, and 6 in the header denote the analysis number.

zonation with lower and lower Ca content from the core toward the rim and complementary enrichment in Fe. Fig. 6 shows TEM–EDX spectra of two analyses at the rim and at the core of a clinopyroxene in the Nakhla sample. One notes the Ca and Fe trend discussed above. The Cu signal is produced by the sample holder and should be considered as blank. The Ga signal is due implantation during the lamaella preparation using a Ga-FIB column. The compositional variation of the mineral lattice does not allow presenting results concerning the composition of individual rock-forming phases in form of averages plus standard deviation. Such a procedure would mess-up the significance of the results, thus not allowing showing evolutionary trends that are indeed geochemically relevant.

Melt inclusions in the augite of the nakhlite meteorites were characterized by a dominant SiO_2-rich phase and different daughter phases. The SiO_2-rich phase was not crystalline, rather vitreous as suggested by SAED patterns. The composition was to be obtained in a certain range (SiO_2 77–88%, Al_2O_3 10–17%, CaO 1%, alkali oxides <5%) that is retained to be representative of the actual sample composition heterogeneity. A possibility to explain sample composition variation is the occurrence of alteration phases. However, the latter

Table 2
Normalized concentration in mass percent of rock-forming phases in a selection of points determined using TEM–EDX in Nakhla sample of Fig. 4

Phase	Silica-rich phase			Clinopyroxene							Cl-apatite	
	1	2	3	1	2	3	4	5	6	7	1	2
SiO_2	76.6	82.2	87.9	47.6	45.8	47.5	48.2	48.5	49.5	45.5	6.0	3.4
Al_2O_3	17.4	15.7	9.5	1.9	1.4	2.6	5.6	5.4	1.9	5.9	<	<
Fe_2O_3	0.6	0.7	0.7	17.6	31.1	16.1	15.9	14.8	17.6	15.0	1.3	0.8
MgO	4.5	<	<	16.8	20.0	17.4	15.5	15.4	16.0	17.5	1.6	<
CaO	0.7	1.1	0.9	16.1	1.2	16.4	14.8	15.5	15.0	16.1	43.9	49.7
MnO	<	<	<	<	0.6	<	<	0.3	<	<	<	<
Na_2O	<	<	1.0	<	<	<	<	<	<	<	<	<
K_2O	0.3	0.4	0.1	<	<	<	<	<	<	<	<	<
P_2O_5	<	<	<	<	<	<	<	<	<	<	44.0	42.4
Cl_2O	<	<	<	<	<	<	<	<	<	<	3.4	3.7

The numbers 1, 2, 3, 4, 5, and 6 in the header denote the analysis number.

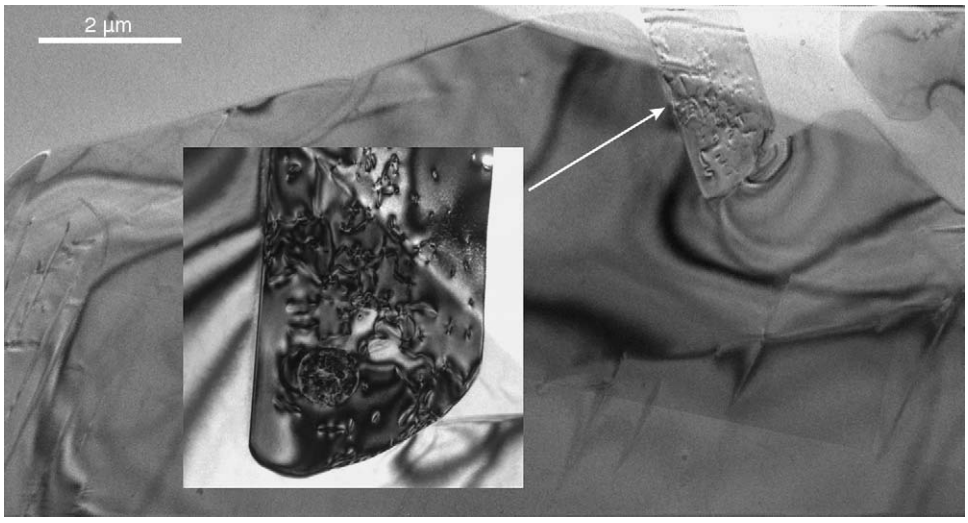

Fig. 4. TEM image of FIB-prepared lamaella where the TEM–EDX determinations have been performed (Table 2). Euhedral chloro-apatite melt inclusion in Nakhla clinopyroxene.

were not observed inside any inclusion in the Nakhla sample, which shows the importance of having access to an image data set.

The issue of goodness of quantitation, i.e. precision and accuracy, is a critical one for this kind of applications. In fact, the most limiting factor is here reliability of results and not detection power, since mineralogical processes can be carefully studied on the basis of the major element content in the minerals. High detection power would be required for trace analysis where trace elements offer a powerful tool for geochemical investigations. In order to carefully assess the thermo-barometric conditions of one rock-forming mineral assemblage one needs to obtain elemental concentration values of small uncertainty or systematic error. Unfortunately, many beam-assisted techniques that are routinely used in the geo-sciences implement semi-quantitative algorithms that cannot provide data with higher accuracy than 10% relative. The precision is typically a function of sample preparation, e.g. surface roughness. As said above, in some case data scatter is due to signal mixing from different mineral phases because the measurement is volume-oriented.

The melt inclusions in olivine were multiphase mainly constituted by a SiO_2-rich phase and augite, and by several euhedral daughter minerals, like low-Ca pyroxene, chloro-apatite, magnetite, Cr-magnetite. The SiO_2-rich phase is vitreous as well as in the inclusions from augite. Determined compositions were varying in amount of constituting oxides: SiO_2 80–89%, Al_2O_3 4–16%, CaO <1%, alkali oxides 2–4%. Intense alteration veins (composed by SiO_2 38–52%, Fe_2O_3 28–35%, Na_2O 15–18% and CaO 1–3%) cut through the host olivine and penetrate the inclusion.

Fig. 7 shows a typical LA–ICPMS intensity signal versus measurement time for Al and Mg, together with their intensity ratio (top panel). In the first 20 s gas blank signal was acquired for background reference. Then the laser beam was delivered onto the sample surface and ablation began on the host mineral. After several seconds (approx. 10 s in the inclusion shown in the figure) the pit was deep enough to begin

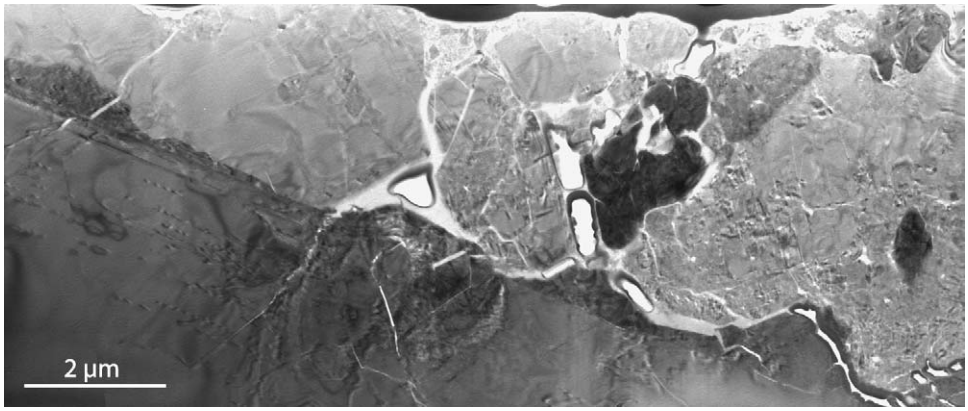

Fig. 5. TEM image of FIB-prepared lamaella where the TEM–EDX determinations have been performed (Table 3). NWA817 melt inclusion in clinopyroxene showing the presence of cavities along the boundary contacts and scattered opaque minerals domains.

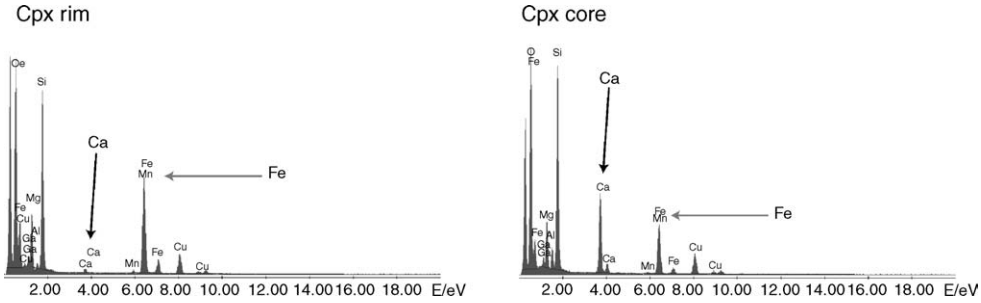

Fig. 6. TEM–EDX spectra of clinopyroxene in the Nakhla sample acquired at the rim and at the core. The Cu signal is produced by the sample holder and should be considered as blank. The Ga signal is due implantation during the lamaella preparation using a Ga-FIB column. Ca and Fe are good markers of the compositional zoning in the lattice of the mineral.

direct ablation of the inclusion. The spot size was initially matched to the inclusion size to obtain optimum sensitivity from the inclusion only. In Fig. 7, Mg and Al are shown as indicators of the inclusion and host during the ablation progression because such elements are differently partitioned in the two phases. When the drilling proceeded through the host clinopyroxene the Al/Mg ratio was approx. 0.4 in the signals. The ratio Al/Mg increased a factor of 4 right during the ablation of the melt inclusion. Therefore, data reduction to quantitate the various elements was targeted to the two separated portions ablated, i.e. the host phase and the inclusion phase. The LA–ICPMS measurements of the melt inclusions in the clinopyroxene indicated an augitic average composition, i.e. in mass percent it resulted to be in the following ranges: SiO_2 49.4–49.6%, Al_2O_3 3.8–4.0%, TiO_2 0.3%, FeO 20.7–21.5%, MnO 0.5%, MgO 9.5–9.9%, CaO 12.8–14.3%, Cr_2O_3 0.2%, NiO 0.01%, Na_2O 0.7%. LA–ICPMS quantitative data were compared to the TEM–EDX semi-quantitative results. Obviously, this comparison was not done on the melt inclusions due to the problems discussed in the introduction and the consequent risk of unrepresentative determination. Rather this was done on the rock-forming phases, as shown in Fig. 8.

In conclusion, the analytical palette of techniques implemented in this work gave access to a complete data set, i.e. geometry, composition and crystallinity of both the augite and olivine hosted inclusion in the two nakhlitic meteorites.

The detailed petrological implications of these data for planetary studies are out of the scope of the present communication and will be discussed in detail elsewhere [14]. However the major outcomes are given in brief. The melt inclusions studied in the minerals augite and olivine of the nakhlite meteorites allowed to formulate hypothesis about the composition of the parent magma and its late evolution in the cooling sequence. The differences in composition between melt inclusions in olivine and augite crystals would suggest a xenocrystic origin for olivine, as speculated previously. Therefore, olivine entrapped a portion of the pristine magmatic pile that is different in location and composition from the one entailed in the augite-hosted inclusions. Only during a later stage, the olivine could migrate into to the final entrapment location across a still molten magmatic pile. This suggests a complex petrogenesis active on Mars.

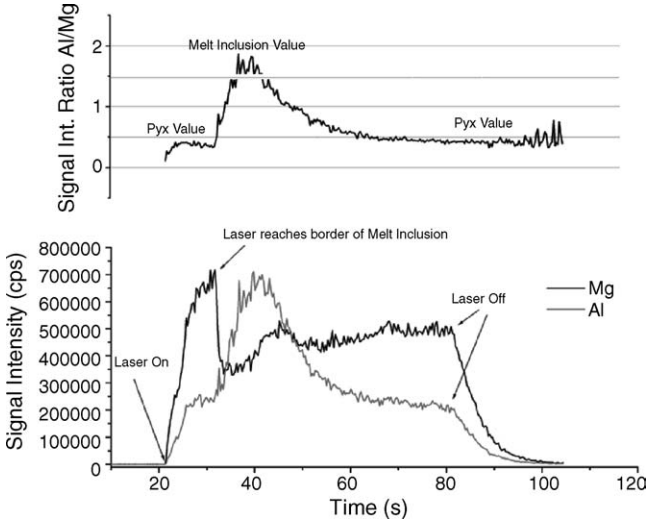

Fig. 7. LA–ICPMS transient signal of the opening of one melt inclusion and Al/Mg ratio showing the evolution of the ablation process, i.e. ablation of embedding host and ablation of melt inclusion.

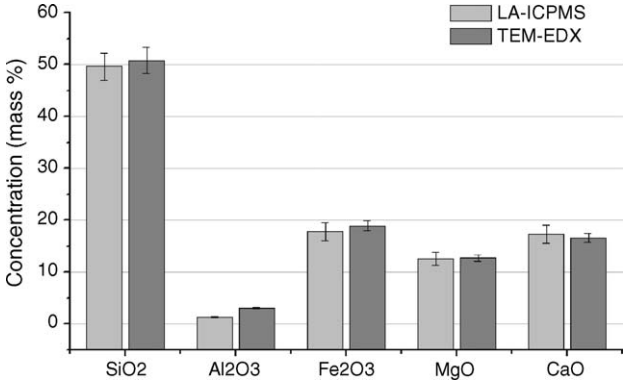

Fig. 8. Comparison of TEM–EDX and LA–ICPMS results obtained for the analysis of a clinopyroxene in a region close to the core. LA–ICPMS was able to detect also minor content of Na, Ti, Mn, and Cr, which could not be detected using TEM–EDX. Uncertainty bars reflect a consistent set of probed regions in the phase (i.e. measurement points in the core).

The daughter minerals association in the inclusions of the Nakhla meteorites is different from that of the inclusions in NWA817 meteorites, i.e. fayalite, hedenbergite and crystallized SiO_2 coexisting with chloro-apatite. Fayalite is the Fe-rich term of olivine solid solution $(Fe, Mg)_2SiO_4$ whereas hedenbergite is the Fe-rich term of the clino-pyroxene solid solution $(Fe, Mg)CaSi_2O_6$. Such an association has been described in lunar rocks and in melt pockets of another group of Martian meteorites, i.e. the shergottites [15–17]. Such a mineralogical association led several workers to claim the breakdown of an iron-rich melt at low pressure at a cooling rate slower than 4 °C/h [18].

However, the SAED patterns collected demonstrated that the SiO_2-rich phase in inclusions from augite in meteorites from North West Africa site (NWA817) is re-crystallized, whereas it is still vitreous in the inclusions from Nakhla sampling site. The fact that the SiO_2-rich phase is re-crystallized is determined by the SAED pattern showing several reflexes, whereas a trapped liquid is expected to be amorphous. This clearly indicated that different post-entrapment evolutions were active for the two nakhlite meteorite sets, the Nakhla and the NWA817 set. Inclusions from NWA817, also characterized by the presence of fractures, might have been altered by exchange with the environment and so partially lost theirs primary characters. Melt inclusions in Nakhla olivine presented alteration veins, which were possibly produced before their landing on Earth [19,20]. If this is the case, this would indicate a alteration stage already on Mars. Melt inclusions in Nakhla augite resulted unaffected by any alteration or modification following the entrapment, and therefore represent the best candidate to indicate the pristine melt composition. The obtained composition is in agreement to those obtained by other authors [21–30].

4. Conclusions

FIB-assisted milling offers exceptional precision in preparing selected areas of a sample for examination by SEM and TEM. Here it was possible to characterize the mineral assemblage in terms of composition, crystallinity and also to acquire SE images at micro- and sub-microscale. The advantage is that one obtains direct access to information on inclusion structure and composition. LA–ICPMS allowed determination of the melt inclusions in mass-oriented mode, whereas the very popular EPMA determination is volume-oriented. This point should not be underestimated in combination with heterogeneous inclusions with irregular shape, fractures or voids. LA–ICPMS could also provide depth-resolved concentration profiles so that one was able to assess the location of differentiated portions or fractures. The obtained data permitted to put further constraints on the reconstruction of the petrogenesis of Mars as well as to speculate about the possibility of a weathering stage during the history of the planet.

Acknowledgements

M.L. Frezzotti (University of Siena) and J.P. Lorand (CNRS Musée National Histoire Naturelle) are kindly acknowledged for productive discussions at various stages of this project. P. Lienemann (EMPA) is acknowledged for discussion during the entire duration of the work. F. “Paco” Alvarez and Ch. Bottali (EMPA) are acknowledged for support on the laser ablation facility. Mrs. T. Lella is acknowledged for logistical support. J. Strobe is acknowledged for providing some rare meteorite samples.

References

[1] D.A. Papanastassiou, G.J. Wasserburg, Geophys. Res. Lett. 1 (1974) 23–26.
[2] R.N. Clayton, T.K. Mayeda, Earth Planet. Sci. Lett. 62 (1983) 1–6.
[3] C.Y. Shih, et al., Geochim. Cosmochim. Acta 46 (1982) 2323–2344.
[4] D.D. Bogard, P. Johnson, Science 221 (1983) 651–654.
[5] H.Y. McSween Jr., Rev. Geophys. 23 (1985) 391–416.
[6] M.E. Varela, G. Kurat, R. Clocchiatti, Miner. Petrol. 71 (2001) 155–172.
[7] R.P. Harvey, H.Y. McSween, Earth Planet. Sci. Lett. 111 (1992) 467–482.
[8] A.H. Treiman, Geochim. Cosmochim. Acta 57 (1993) 4753–4767.
[9] R.P. Taylor, S.E. Jackson, H.P. Longerich, J.D. Webster, Geochim. Cosmochim. Acta 61 (1997) 2559–2567.
[10] W.E. Halter, Th. Pettke, Ch.A. Heinrich, B. Rothen-Rutishauser, Chem. Geol. 183 (2002) 63–86.
[11] Th. Pettke, W. Halter, J.D. Webster, M. Aignes-Torres, Ch.A. Heinrich, Lithos 78 (2004) 333–361.
[12] C.A. Heinrich, Th. Pettke, W.E. Halter, M. Aigner-Torres, A. Audetat, D. Günther, B. Hattendorf, D. Bleiner, M. Guillong, I. Horn, Geochim. Cosmochim. Acta 67 (2003) 3473.
[13] D. Bleiner, GIT Lab. J. 8 (2004) 40.
[14] M. Macri’, PhD Thesis, University of Rome, in preparation.
[15] T.J. McCoy, M. Wadhwa, K. Keil, Geochim. Cosmochim. Acta 63 (1999) 1249–1262.
[16] A.E. Rubin, P.H. Warren, J.P. Greenwood, R.S. Verish, L.A. Leshin, R.L. Hervig, R.N. Clayton, T.K. Mayeda, Geology 28 (2000) 1011–1014.
[17] T. Mikouchi, Antarctic Meteorite Res. 14 (2001) 1–20.
[18] D.H. Lindsley, J.J. Papike, A.E. Bence, Lunar Sci. III (1972) 483–485 (abs.).
[19] T.E. Bunch, A.M. Reid, Meteorites 10 (1975) 303–315.
[20] J.R. Ashworth, R. Hutchison, Nature 256 (1975) 714–715.
[21] A.H. Treiman, Geochim. Cosmochim. Acta 50 (1986) 1061–1070.
[22] J. Longhi, V. Pan, The parent magmas of the SNC meteorites, in: Proceedings of the 19th Lunar and Planetary Science Conference, 1989, pp. 451–464.
[23] R.P. Harvey, H.Y. McSween, Earth Planet. Sci. Lett. 111 (1992) 467–482.
[24] K. Kaneda, G. McKay, L. Le, Lunar Planet. Sci. XXIX (1998).
[25] A.H. Treiman, C.A. Goodrich, Lunar Planet. Sci. XXXII (2001).
[26] E.P. Vicenzi, P.J. Heaney, Lunar Planet. Sci. XXX (1999).
[27] P.J. Heaney, E.P. Vicenzi, L.A. Giannuzzi, K.J.T. Livi, Am. Miner. 86 (9) (2001) 1094–1099.
[28] L.F. Dobrzhinetskaya, H.W. Green, M. Weschler, M. Darus, Y.C. Wang, H.J. Massonne, B. Stöckhert, Earth Planet. Sci. Lett. 210 (2003) 399–410.
[29] C. Viti, M.L. Frezzotti, Lithos 55 (2001) 125–138.
[30] M.L. Frezzotti, Lithos 55 (2001) 273–299.